Precambrian Research 280 (2016) 1–13

Contents lists available at ScienceDirect

Precambrian Research

journal homepage: www.elsevier.com/locate/precamres

Decoupled sources of the 2.3–2.2 Ga Yuanjiacun banded iron formation: Implications for the Nd cycle in Earth's early oceans

Changle Wang [a,b], Kurt O. Konhauser [c], Lianchang Zhang [a,*], Mingguo Zhai [a], Wenjun Li [a]

[a] Key Laboratory of Mineral Resources, Institute of Geology and Geophysics, Chinese Academy of Sciences, Beijing 100029, China
[b] University of Chinese Academy of Sciences, Beijing 100049, China
[c] Department of Earth and Atmospheric Sciences, University of Alberta, Edmonton, Alberta, Canada

ARTICLE INFO

Article history:
Received 2 June 2015
Revised 17 April 2016
Accepted 27 April 2016
Available online 4 May 2016

Keywords:
Yuanjiacun
Archean and Paleoproterozoic
Seawater
Neodymium
BIF

ABSTRACT

The recognized worldwide gap in BIF deposition between 2.4 and 2.0 billion years ago has long been considered as an obstacle to fully determining the geochemical composition of seawater at that time. However, the recently dated 2.3–2.2 Ga Yuanjiacun banded iron formation (BIF) in the North China Craton (NCC) offers a possibility to redress these uncertainties. Shale-normalized rare earth element-yttrium (REE + Y) patterns of the BIF and interlayered meta-chert samples show features characteristic of other Archean and Paleoproterozoic BIFs, with HREE enrichment relative to LREE, positive La and Eu anomalies, and superchondritic Y/Ho ratios comparable to modern seawater. Very low Al_2O_3 (<0.5 wt %) and high field strength elements (HFSE) concentrations (<10 ppm) indicate an essentially detritus-free depositional setting, while positive Eu anomalies are attributed to an imprint of high-temperature hydrothermal fluids. Sm–Nd isotopic features further point to two periodically interacting water masses controlling the deposition of the BIF. The first is seafloor-vented hydrothermal fluids ($\varepsilon_{Nd}(t) \sim +3.5$) derived from interaction with a depleted mantle source and associated with high Fe fluxes. The second is ambient surface seawater ($\varepsilon_{Nd}(t) \sim -2.4$), which obtained its signature through weathering of the nearby landmasses and associated with high Si fluxes. Our findings suggest that the REE budget of the oceans prior to 2.3 Ga was generally dominated by hydrothermal circulation of seawater through depleted mantle-derived source rocks. However, where evolved local continental crust and/or an enriched mantle source were present, this positive mantle Nd signal became discernible in the BIFs. By comparing the Nd isotopic features of similar aged BIFs and marine carbonates, it is concluded that similar to modern oceans, the early Precambrian ocean was not well-mixed with respect to its Nd isotopic composition.

1. Introduction

Banded iron formations (BIFs) are amongst the most common types of chemical sediments precipitated during the Archean and early Paleoproterozoic (Klein, 2005), and their trace element and isotopic features have been used with great success as proxies for understanding the chemical composition of seawater from which the sediments precipitated (Bau et al., 1997; Frei and Polat, 2007; Konhauser et al., 2009; Bekker et al., 2010). The rare earth elements (REEs) are particularly useful for such studies due to their coherent behavior in geochemical systems. Moreover, with few exceptions, shale-normalized (data normalized against Post-Archean Australian Shale, PAAS, from McLennan, 1989) REE + Y patterns of detritus-poor pre-Mesoproterozoic BIFs are remarkably similar to those of Archean–Paleoproterozoic marine carbonates (Kamber and Webb, 2001; Bau and Alexander, 2006) and modern seawater, exhibiting positive La, Gd and Y anomalies and enrichment of the heavy REE over the light REE (Bau and Dulski, 1996; Bolhar et al., 2004; Planavsky et al., 2010; Mloszewska et al., 2012, 2013). The most salient differences between the REE + Y distribution in modern seawater and BIFs are that the latter have consistently positive Eu anomalies and lack the characteristic strongly negative Ce anomalies of modern seawater. The former indicates significant contributions from high-temperature (>250 °C) hydrothermal fluids emanating from submarine venting systems (Bau and Dulski, 1999), while the latter reflects a relatively reducing oceans (Holland, 1984).

This approach, coupled with Nd isotope systematics, has also been used to constrain the relative magnitude of continental and hydrothermal fluxes to the oceans (Miller and O'Nions, 1985;

* Corresponding author.

http://dx.doi.org/10.1016/j.precamres.2016.04.016
0301-9268/

Alibert and McCulloch, 1993; Frei et al., 2008; Haugaard et al., 2013). Considering the close association of REE with Fe in marine and freshwater environments, the similar Fe/Nd rations ($\approx 10^5$) in BIFs and modern hydrothermal waters suggest that REE and iron were derived from the same source (Jacobsen and Pimentel-Klose, 1988a). Based on this premise, previous workers have calculated the mass fraction of Fe derived from different sources by conservatively mixing a hydrothermal end-member possessing a depleted-mantle Nd isotope ratio ($\varepsilon_{Nd}(t) > 0$) with a river/ambient seawater end-member which possesses a continental Nd isotope signature ($\varepsilon_{Nd}(t) < 0$) (e.g., Alibert and McCulloch, 1993; Bau et al., 1997; Døssing et al., 2009). Despite some limitations due to possible metamorphic disturbance (Miller and O'Nions, 1985) or different geochemical behaviors of Fe and Nd (Alexander et al., 2008), $\varepsilon_{Nd}(t)$ values may still be used to infer the source of Fe other than REE to contemporary seawater.

There is a recognized lack of BIF between ~2.4 and ~2.0 Ga (Isley and Abbott, 1999; Bekker et al., 2010), but not a complete absence. In this regard, we firstly reported the Sm–Nd isotopic data for samples from the 2.3–2.2 Ga Yuanjiacun BIF and intercalated ferruginous quartzite (recrystallization from chert) of the Lüliang Group, NCC. The distribution of REE and Y in this BIF has been previously described (Wang et al., 2014a, 2015a) and displayed no peculiarities when compared to other BIFs worldwide, except for the presence of scattered Ce anomalies in some samples. Major and trace elements whole-rock geochemical analyses have also been carried out on the quartzite to evaluate its origin. Furthermore, in conjunction with previously published Sm–Nd isotopic data for other Archean and Paleoproterozoic BIFs, we reexamine the estimates of the relative balance between continental and mantle-derived sources of REE and iron, and then re-evaluate the Nd isotopic evolution in the oceans during the period.

2. Geological setting

The North China Craton (NCC) in China is widely recognized as one of the oldest cratons in the world, and it hosts large amounts of Archean BIFs. The basement of the NCC can be divided into the Eastern and Western Blocks which are separated by the intervening Trans-North China Orogen (TNCO, Zhao et al., 2005). The Lüliang Complex is located in the western portion of the TNCO, where a large number of Paleoproterozoic supracrustal rocks and granitoid intrusions are exposed (Fig. 1). These supracrustal rock sequences can be divided into four main groups, comprising (from bottom to top) the Jiehekou, Lüliang, Yejishan, and Heichashan or Lanhe groups (Fig. 2). These sequences were intruded by the 2182–2151 Ma Guandishan–Chijianling TTG gneiss and the ~1800 Luyashan charnockite (Yu et al., 1997a; Geng et al., 2000, 2004; Wan et al., 2000, 2006; Zhao et al., 2008; Liu et al., 2009; Xia et al., 2009).

The Lüliang Group is found only in the Jinzhouyu area and comprises greenschist- to amphibolite-facies metamorphosed sedimentary and volcanic rocks, with clastic meta-sedimentary rocks and BIF in the lower sequence and metamorphosed volcanic rocks in the upper part of the sequence (Yu et al., 1997a; Liu et al., 2012). These sequences are subdivided into four major units: the lower Yuanjiacun Formation, the middle Peijiazhuang and Jinzhouyu Formations, and the upper Dujiagou Formation. The Yuanjiacun Formation exposed in the Yuanjiacun area is a greenschist-facies metasedimentary sequence, which is represented by well-bedded chlorite schists, sericite-chlorite phyllites, sericite schists, quartzite, BIF and minor carbonaceous chlorite schists (Fig. 3a). The Yuanjiacun Formation was unconformably overlain by the Middle Cambrian limestone (Tian et al., 1986), at the base of which occur two layers of conglomerate-type BIF approximately 2–14 m stratigraphically apart (Fig. 3b). The Yuanjiacun BIF is commonly found interbedded with chlorite schists and sericite schists, and the contacts are sharp, straight and well-defined with no sign of any grading, erosion or intermixing (Fig. 3b). Igneous rocks exposed in the study area consist predominantly of metamorphic diabase dykes, which commonly intrude into the BIF and associated clastic meta-sediments with widths varying from several meters to more than 100 meters. From north to south, the diabase content increases and its width becomes larger. There are no features indicative of alteration or contact metamorphism due to the intrusion of the diabase.

The Yuanjiacun BIF is distributed in a NNE–NEE orientation, extending 20.5 km in length and 5.8 km in width. Fig. 3(a) only depicts the middle part of this long belt where the BIF is well developed and exposed. It strikes N–S and N–NE, dips steeply SE or E at 70–80° (Fig. 3a). Individual layers of the BIF vary commonly from less than 1 m to tens of meters in the section (Fig. 3b). Post-depositional deformation is generally minimal, but with intense folds developed locally. Faults that occur in the study area are interpreted as post-depositional with little effects on the BIF.

Yu et al. (1997b) obtained single-grained zircon U–Pb ages of 2051 ± 68 Ma and 2099 ± 41 Ma from mafic meta-volcanics in the Jinzhouyu Formation and meta-rhyolites in the Dujiagou Formation, respectively. In addition, three ages were reported by Geng et al. (2000, 2008), including zircon U–Pb ages of 2360 ± 95 Ma from the interlayered intermediate-felsic volcanic tuff in the Jinzhouyu Formation, 2175 Ma from the meta-rhyolites in the Dujiagou Formation, and a whole rock Sm–Nd isochron age of 2351 ± 56 Ma for mafic meta-volcanics in the Jinzhouyu Formation. Liu et al. (2012) reported a LA-ICP-MS U–Pb zircon age of 2213 ± 47 Ma from a mafic volcanic rock in the Jinzhouyu Formation. Most recently, Liu et al. (2014) also obtained crystallization ages of 2209–2178 Ma and 2196 ± 20 Ma of the mafic meta-volcanic rocks from the Jinzhouyu and Dujiagou formations, respectively. Moreover, Wang et al. (2015b) conducted a geochronological study on the meta-sedimentary rocks intercalated with the Yuanjiacun BIF and obtained the youngest zircon age group of ~2372–2348 Ma. Considering that there exists a potential depositional gap characterized by a disconformity between the Peijiazhuang and Jinzhouyu formations (Tian et al., 1986; Yu et al., 1997a), we propose that the age of the Yuanjiacun Formation should date to the Paleoproterozoic (2.3–2.2 Ga), representing the depositional age of the Yuanjiacun BIF.

3. Samples description and analytical methods

A large number of Precambrian BIF samples have been analyzed (e.g., Shimizu et al., 1990; Bau et al., 1997), but only a very few are found to provide the desired information, due, for example, to possible contamination with clastic detritus or post-depositional metamorphic resetting of the isotopic system of the chemical sediment. In this study, we exploit the sample set and the results of previous work (e.g., Frei and Polat, 2007; Alexander et al., 2008, 2009; Frei et al., 2008) on the REE and Y geochemistry and Sm–Nd isotopic features of the BIFs. Following a very strict screening procedure, we could select the best representative samples with reliable $\varepsilon_{Nd}(t)$ values of each BIF (see Appendix Table).

The samples have to meet the following chemical criteria: (i) Very low contents of Al_2O_3 (<0.5 wt%) and low concentrations of incompatible elements (Th, Hf, Zr, Sc, etc.) because these elements are typically associated with detrital aluminosilicates and previous studies (Dymek and Klein, 1988; Bau, 1993; Bolhar et al., 2004; Alexander et al., 2009; Haugaard et al., 2013) have shown that even small contributions of crustal detritus were sufficient to swamp the REE distribution and dominate the Nd budget of the BIF. (ii) Very low Na content, indicating the absence of minor amounts of

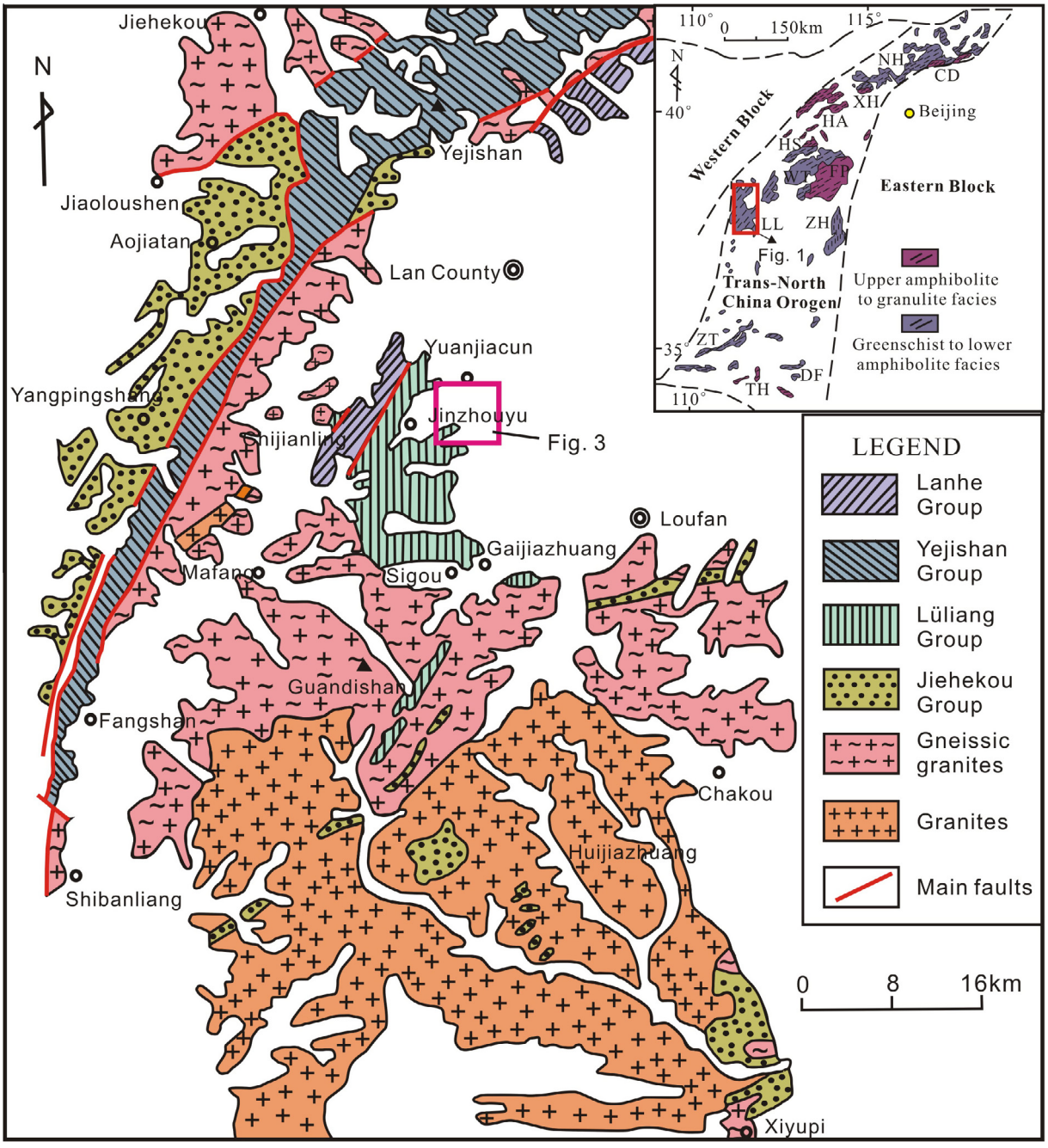

Fig. 1. Geological sketch of the Paleoproterozoic Lüliang Complex (modified from Wan et al., 2000). The insert map shows the location of the Lüliang Complex in the North China Craton (revised after Zhao et al., 2005). Abbreviations for metamorphic complexes: CD, Chengde; DF, Dengfeng; FP, Fuping; HA, Huai'an; HS, Hengshan; LL, Lüliang; NH, Northern Hebei; TH, Taihua; WT, Wutai; XH, Xuanhua; ZH, Zanhuang; ZT, Zhongtiao.

riebeckite because the Na-bearing amphibole riebeckite is found to accompany disturbed Sm–Nd isotopic compositions in the Hamersley BIFs (Alibert and McCulloch, 1993). (iii) Clear seawater-like REE + Y patterns, i.e., LREE depletion relative to HREE with positive La and Gd anomalies and superchondritic Y/Ho ratios (>26) which indicate that the REE distribution in the BIF samples has not been modified by post-depositional processes (Bau and Dulski, 1996). Moreover, anomalously wide variations in $\varepsilon_{Nd}(t)$ have not been observed in BIF samples that possess these typical REE contributions (Bau et al., 1997; Frei and Polat, 2007; Alexander et al., 2009), suggesting that these BIF samples could represent the best archives of coeval Precambrian seawater $^{143}Nd/^{144}Nd$. (iv) Some samples, with anomalous $\varepsilon_{Nd}(t)$ values, are ascribed obviously to later metamorphic effects (e.g., Isua BIF, Shimizu et al., 1990; Hamersley BIFs, Alibert and McCulloch, 1993), and thus have been precluded from the following discussion. Nevertheless, any attempt at reconstructing the Nd isotopic evolution of Precambrian seawater is hampered by the poor resolution in depositional ages of a few BIFs. In this regard, we recalculate the $\varepsilon_{Nd}(t)$ values of some BIFs based on their available age dates (Bekker et al., 2010; Wang et al., 2014b) (Appendix Table).

For the Yuanjiacun BIF, twelve bulk-BIF samples were chosen from a previous sample set (Wang et al., 2014a, 2015a) to conduct Sm–Nd isotopic analyses. Mineralogical assemblages observed in all samples are composed mainly of hematite/magnetite and quartz, with lesser amounts of Fe-rich silicates (e.g., stilpnomelane)

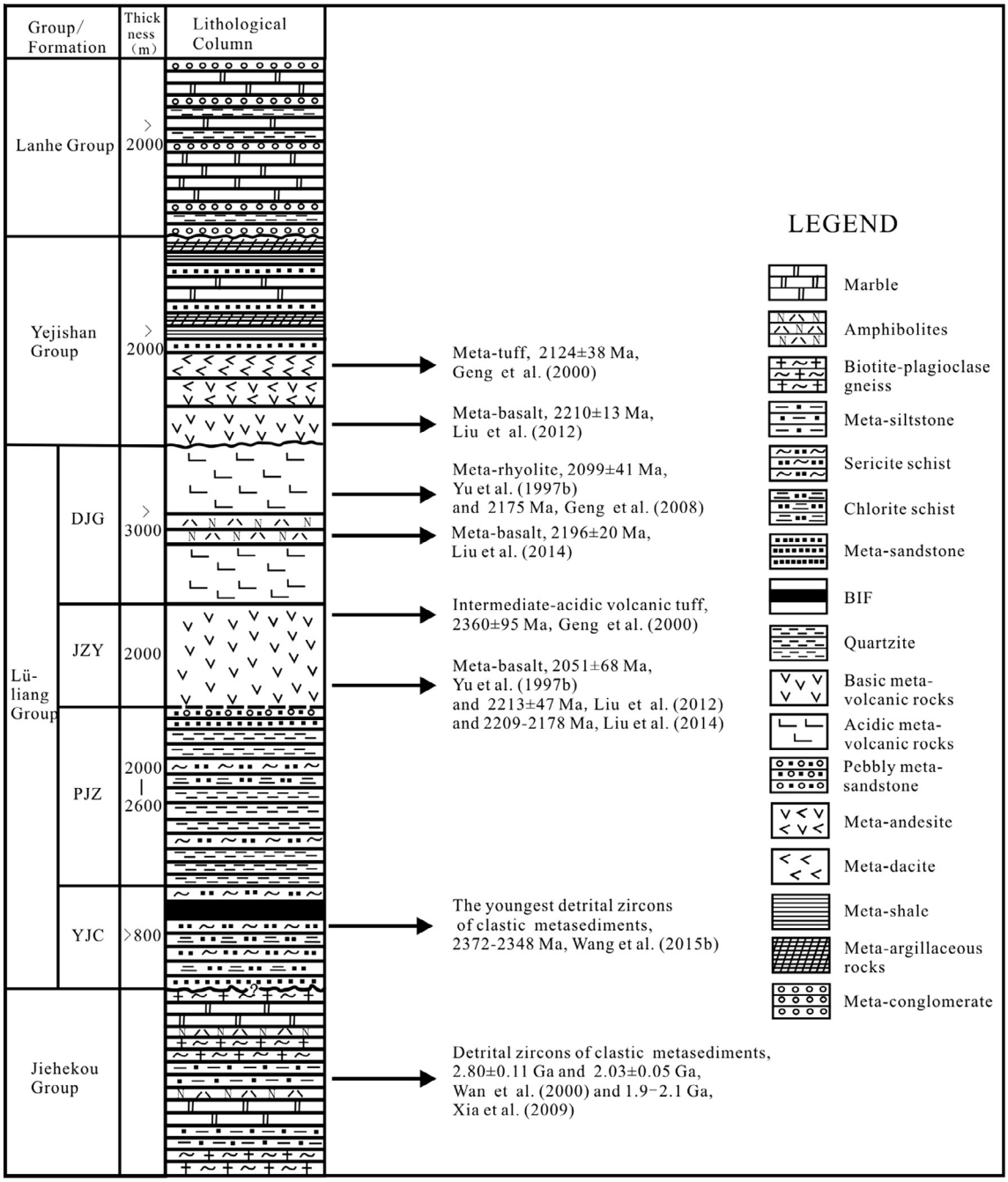

Fig. 2. Stratigraphic column showing Group and Formation names for different rock assemblages in the Lüliang Complex (modified after Tian et al., 1986). Abbreviations for formation names: YJC, Yuanjiacun Formation; PJZ, Peijiazhuang Formation; JZY, Jinzhouyu Formation; DJG, Dujiagou Formation.

and carbonates (e.g., ankerite). Six ferruginous quartzite samples interlayered with the BIF were also collected for relevant geochemical analyses. They consist predominantly of quartz (>90%) and minor hematite. All samples were free of post-diagenetic hydrothermal alteration (as evident by the absence of veins and alteration minerals), and fresh unweathered samples were subsequently crushed.

All geochemical and Sm–Nd isotopic analyses were conducted at the Institute of Geology and Geophysics, Chinese Academy of Sciences in Beijing. Major element oxides were analyzed using XRF-1500 X-ray fluorescence (XRF) with RSD between 0.1% and 1%. Trace element (including REE + Y) concentrations were analyzed with an inductively coupled plasma-mass spectrometer (ICP-MS) (Element, Finnigan MAT) using solution methods. The accuracy on the measured concentrations is within 5–10%. Shale-normalized REE patterns (subscript "SN", normalized to the Post-Archean Australian shale (PAAS), after McLennan (1989)) are presented for all BIF whole rock samples. Because the chemical behavior of Y is similar to those of the REE, Y is inserted between Dy and Ho based on its ionic radius. Thus, Y and the REE are considered together (Bau and Dulski, 1996).

For Nd isotope analyses of the BIF and ferruginous quartzite samples, about 150–300 mg of powder was weighed into 7 ml SavillexTM Teflon beakers, and appropriate amounts of mixed ^{149}Sm–^{150}Nd spikes were added. The samples were dissolved using a mixed acid of 2 ml HF and 0.2 ml $HClO_4$. In order to make them totally dissolved, the beakers are then put on a hotplate at 120 °C for more than one week. After that, the solutions were dried on

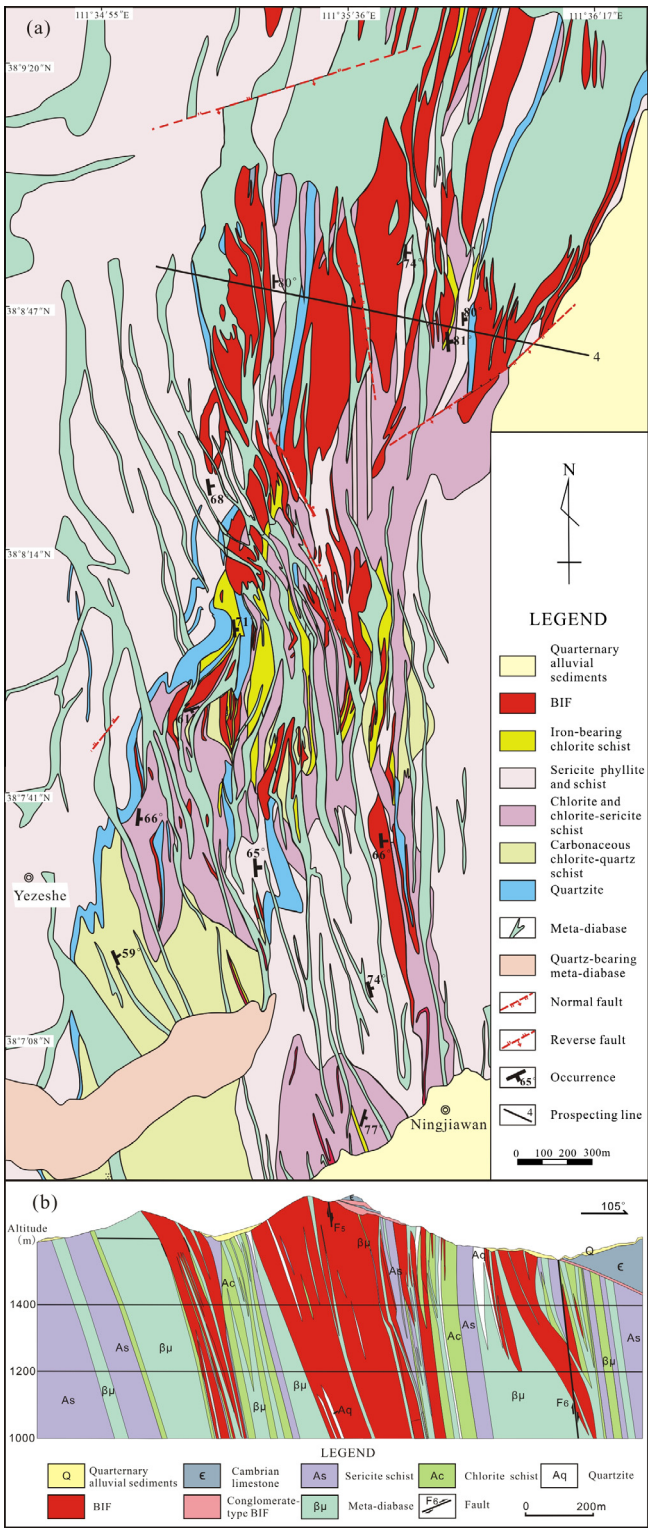

Fig. 3. (a) Geological map of the Yuanjiacun BIF, showing the distribution of the Yuanjiacun BIF and associated clastic and chemical meta-sediments (modified from Tian et al., 1986). (b) Profile of IV prospecting line in the Yuanjiacun area, showing the relationship between the Yuanjiacun BIF and associated meta-sedimentary rocks (modified from Tian et al., 1986).

hotplate at 130–180 °C to remove the HF and $HClO_4$. The sample residues were re-dissolved in 4 ml of 6 M HCl, and then dried down again. Finally, the samples were dissolved in 5 ml of 3 M HCl. The procedures for chemical separation and isotopic measurement followed Chu et al. (2009).

The Sm–Nd isotopic analyses were conducted using a Finnigan MAT 262 thermal ionization mass spectrometer. Measured $^{143}Nd/^{144}Nd$ ratios were corrected for mass-fractionation using $^{146}Nd/^{144}Nd = 0.7219$. During the period of data collection, the measured values for the JNdi-1 Nd standard was $^{143}Nd/^{144}Nd = 0.512113 \pm 11$ (2σ, $n = 4$). The USGS reference material BCR-2 was measured for Sm–Nd isotopic composition to monitor the accuracy of the analytical procedures.

All the initial $^{143}Nd/^{144}Nd$ values of the BIF and associated quartzite samples are calculated using an age of 2.3 Ga, which is considered a probable depositional age for the Yuanjiacun BIF (See the text). T_{DM} ages were calculated according to DePaolo (1981).

4. Results

4.1. Major and trace elements

Element concentrations for the BIF samples are typical of other Archean and Paleoproterozoic BIFs, with SiO_2 (average of 48.9 wt%) and Fe_2O_3 (average of 49.4 wt%) dominating the major element abundances (Wang et al., 2014a, 2015a). Al_2O_3, TiO_2, MnO, and P_2O_5 are present only in trace amounts (<0.5 wt%), and Na_2O and K_2O are absent or not measurable. Immobile trace element concentrations (e.g., Zr, Hf, Sc) in the samples are also low (<10 ppm), consistent with the Al_2O_3 content of the samples. REE + Y patterns of all samples, normalized against PAAS, are very similar to each other except for a wide range of LREE/HREE ratios (Fig. 4A). They are characterized by depletion of LREE relative to HREE with positive La, Eu, and Gd anomalies and superchondritic Y/Ho ratios. With the exception of the positive Eu anomaly, which is likely attributed to high-temperature hydrothermal fluids, these features are typical of modern seawater (Derry and Jacobsen, 1990; Bau and Dulski, 1996; Bolhar et al., 2004; Pecoits et al., 2009).

Ferruginous quartzite samples consist mostly of SiO_2 (90.0–98.6 wt%) and $Fe_2O_3^T$ (total iron as Fe_2O_3) (0.84–9.33 wt%), and the concentrations of major elements other than Si and Fe are very low (<0.3 wt%) (Table 1). Trace elements (e.g., Zr, Hf) typically occur in low concentrations (<8 ppm). These features argue against detrital contamination during their precipitation. The total REE and Y concentrations (ΣREY) of all samples are relatively high, ranging from 29.2 to 60.8 ppm. Shale-normalized REE + Y patterns exhibit positive La anomalies (the combination of $(Ce/Ce^*)_{SN} < 1$ and $(Pr/Pr^*)_{SN} \approx 1$ indicates a positive La anomaly; Bau and Dulski, 1996) and Eu anomalies (1.31–1.77), as well as slight HREE enrichments relative to LREE ($(La/Yb)_{SN} = 0.68–0.92$), except for one samples (WYJ-3) displaying a nearly flat REE pattern (Fig. 4B). Yttrium is significantly enriched relative to Ho, yielding slightly superchondritic Y/Ho ratios (29–32). There is a subtle correlation ($R^2 = 0.65$) between ΣREY and Fe_2O_3, suggesting that REEs are predominantly hosted by iron oxides rather than other phases (silicates?).

Compared to the Yuanjiacun BIF (Wang et al., 2014a, 2015a), the quartzite samples are characterized by low contents of Fe_2O_3 and high concentrations of SiO_2 and ΣREY. However, nearly identical REE patterns and mineral assemblages observed between them support a purely chemical origin for the quartzite (totally recrystallization from chert), which more likely equals a highly silica-rich end-member (i.e. silica-rich bands) of the BIF.

4.2. Sm–Nd isotopes

Sm–Nd isotopes and concentrations of these elements in the Yuanjiacun BIF and associated quartzite samples are presented in Table 2. Neodymium and Sm concentrations in the studied BIF samples range from 0.13 to 2.98 ppm and from 0.04 to 0.59 ppm,

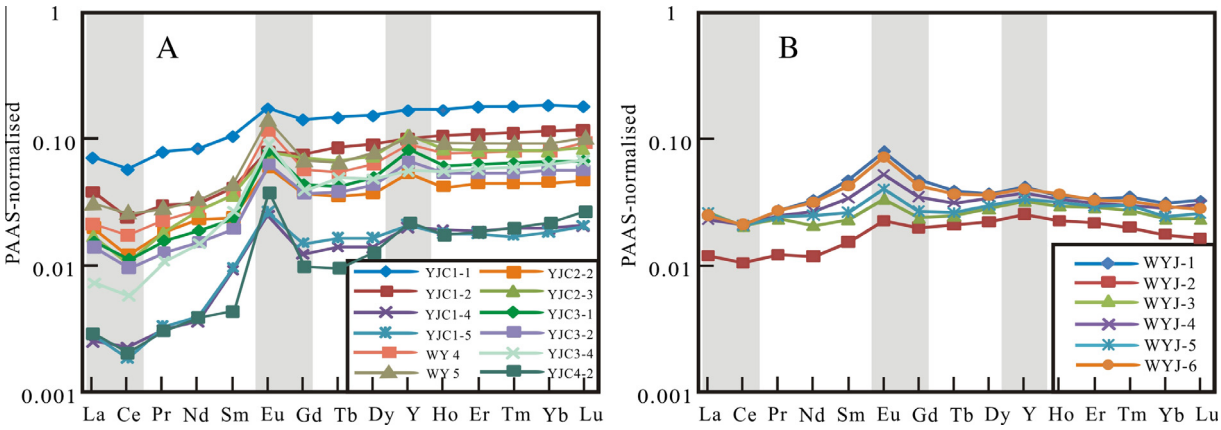

Fig. 4. PAAS-normalized REE + Y diagram of the selected Yuanjiacun BIF (A) (Wang et al., 2014a, 2015a) and associated ferruginous quartzite (B) samples.

respectively. The Sm–Nd isotope data of the BIF plot along a correlation line in a conventional isochron diagram (Fig. 5A) with a slope corresponding to an apparent age of 2335 ± 110 Ma (MSWD = 2.3) with an initial ε_{Nd} value of +0.6. Similarly, the quartzite samples define an array (Fig. 5B) corresponding to an age of 2415 ± 110 Ma (MSWD = 1.6) with an initial ε_{Nd} value of −3.7. These two apparent ages predate the depositional age (2.3–2.2 Ga) of the BIF, and thus the correlation lines likely represent mixing lines. Significantly, these lines do not show convergence at some time younger than ~2.3 Ga, suggesting that post-depositional metamorphism did not induce re-equilibration of the Nd isotopic system. Moreover, the distributions of REY in the BIF and quartzite show characteristic features of modern seawater, and it is highly likely that these characteristics could be retained or generated during pronounced post-depositional input or loss of REEs (Bau et al., 1997). In addition, due to the large size of the whole-rock samples analyzed, small-scale migration of REE had no important impact on the $\varepsilon_{Nd}(t)$ values (Bau and Dulski, 1996). Therefore, it can be concluded that the studied samples have remained closed since shortly after deposition, and that the observed $\varepsilon_{Nd}(t)$ variance among samples reflects primary information at the time of deposition.

The Sm–Nd isotope data of the BIF and quartzite samples are clearly different in that the $\varepsilon_{Nd}(t)$ values are positive (+0.6 to +1.8), for the former, whereas they are consistently negative (−1.6 to −2.5) for the latter. The T_{DM} ages for the quartzite samples (average values of ~2.9 Ga) are older than those of the BIF samples (average values of ~2.7 Ga). The mixing relationship in the BIF is best illustrated in Fig. 6(A), where SiO_2/Fe_2O_3 ratios are plotted against the $\varepsilon_{Nd}(t = 2300\ Ma)$ values. There is a pronounced negative correlation ($R^2 = 0.91$) between these two parameters which indicates the mixing of two sources. The high $\varepsilon_{Nd}(t)$ values are defined by the iron-rich end-member. Interestingly, a reverse correlation is depicted by data of $\varepsilon_{Nd}(t)$ values and Fe_2O_3 contents for the quartzite samples ($R^2 = 0.86$) (Fig. 6B).

5. Discussion

5.1. Inferences for the source of iron and REEs

The relatively low detrital contribution to the Yuanjiacun BIF and ferruginous quartzite samples renders them suitable as archives for the composition of seawater from which BIF precipitated. The positive, depleted mantle-like $\varepsilon_{Nd}(t)$ values for the Yuanjiacun BIF, coupled with other geochemical characteristics, such as positive Eu anomalies (Wang et al., 2014a, 2015a), point to a significant mantle component, likely to be of a high-T hydrothermal origin. Moreover, the positive correlation ($R^2 = 0.98$) between Fe_2O_3 and the magnitude of the Eu anomaly in the quartzite samples reflect the fact that iron was closely related to strongly reduced high-T hydrothermal bottom waters, a feature that was pointed out by Bolhar et al. (2004) and Frei and Polat (2007). Nevertheless, the consistently negative $\varepsilon_{Nd}(t)$ values of the quartzite indicate that REEs were initially supplied by continental runoff. However, this may be an oversimplification because PAAS-normalized REE + Y patterns of these samples (Fig. 4) in essence show a distinct seawater signature imprinted by high-T hydrothermal fluids. Hence, pure BIFs and ferruginous quartzite are themselves best described as mixtures of these two components, which is further exemplified by the correlation between initial ε_{Nd} values and SiO_2/Fe_2O_3 ratios or Fe_2O_3 concentrations (Fig. 6A and B).

The combined interpretation of these two figures implies that for the Yuanjiacun BIF, the iron is associated with a significantly depleted source (extrapolated $\varepsilon_{Nd}(t)$ value of +3.5), whereas the Si-rich source, as best reflected by ferruginous quartzite due to high contents of silica (>90 wt%), is characterized by an enriched Nd isotopic signature (extrapolated $\varepsilon_{Nd}(t)$ value of −2.4). In addition, geochemistry and Nd isotopic data of fine-grained clastic meta-sediments interbedded with the Yuanjiacun BIF can provide further source information (Wang et al., 2015b). These meta-sediments consist mainly of meta-arenites and meta-pelites. The meta-pelite samples can be divided into two types: low-Al and high-Al. The Al increase occurred at expense of iron-rich phases (mainly hematite). The low-Al meta-pelites show intermediate compositions between the normal pelite and BIF samples (Wang et al., 2015b), which is to be expected from their hybrid chemical composition and Nd isotopic features. Therefore, consistently positive $\varepsilon_{Nd}(t)$ values and a positive correlation between the $\varepsilon_{Nd}(t)$ values and Fe_2O_3 ($R^2 = 0.69$) in the low-Al meta-pelite samples also suggest that the Fe was sourced from depleted hydrothermal fluids from a MORB-type setting.

We preferentially interpret these two decoupled end-members to represent seafloor high-T hydrothermal fluids that percolated through mid-ocean ridge-type basalts (MORB) and the ambient (i.e., surface) seawater, respectively, in the Yuanjiacun basin during BIF deposition. If this was the case, the Nd isotopic composition of hydrothermal input can be approximated with that of MORB-source mantle (Kamber and Webb, 2001), which at present has an average $\varepsilon_{Nd}(t)$ value of approximately +10. If a linear isotope evolution is assumed for the MORB-source mantle, a hydrothermal input ~2.3 Ga ago would have had a $\varepsilon_{Nd}(t)$ value of +5.1. However, other models for Nd isotope evolution of the MORB-source mantle predict that the $\varepsilon_{Nd}(t)$ values of hydrothermal sources could have been as low as +2 (Nägler and Kramers, 1998). Given this situation, the inferred $\varepsilon_{Nd}(t)$ value is approximately +3.1, which is

Table 1
Major elements (wt%) and selected trace elements (ppm) of the ferruginous quartzites interbedded with the Yuanjiacun BIF.

Sample	WYJ-1	WYJ-2	WYJ-3	WYJ-4	WYJ-5	WYJ-6
SiO_2	90.0	98.6	97.0	94.2	95.6	90.9
TiO_2	0.01	0.01	0.01	0.02	0.01	0.01
$Fe_2O_3^T$	9.33	0.84	1.93	5.24	3.75	8.45
Al_2O_3	0.22	0.07	0.12	0.15	0.13	0.17
MnO	0.01	0.00	0.01	0.01	0.01	0.01
MgO	0.11	0.10	0.13	0.10	0.11	0.1
CaO	0.06	0.04	0.05	0.04	0.04	0.04
Na_2O	0.06	0.07	0.08	0.06	0.07	0.06
K_2O	0.02	0.02	0.02	0.02	0.01	0.03
P_2O_5	0.02	0.02	0.02	0.03	0.03	0.02
LOI	0.18	0.08	0.13	0.10	0.12	0.14
Total	100.01	99.86	99.49	99.93	99.85	99.94
Li	5.02	0.37	1.36	3.01	1.89	4.67
Be	0.14	0.08	0.11	0.13	0.12	0.14
Sc	0.87	0.80	0.67	0.75	0.81	0.78
V	12.9	4.83	5.95	9.56	6.62	11.0
Cr	34.2	11.2	24.9	31.4	28.8	33.5
Co	4.66	3.85	5.60	3.87	4.06	5.13
Ni	18.0	14.7	17.7	17.8	17.7	18.0
Cu	6.49	3.96	5.53	6.02	5.94	6.37
Zn	0.59	1.03	1.12	0.78	1.25	1.17
Ga	0.34	0.07	0.24	0.31	0.26	0.33
Rb	0.96	1.01	1.15	0.87	1.23	1.08
Sr	3.32	4.63	5.18	3.62	4.11	5.07
Zr	7.42	2.24	2.58	2.12	3.05	2.88
Nb	0.54	0.07	0.05	0.17	0.33	0.41
Cs	0.08	0.07	0.21	0.13	0.07	0.09
Ba	2.39	0.20	1.29	1.79	1.53	2.08
La	9.67	4.49	9.89	8.71	9.75	9.44
Ce	16.2	8.26	16.1	16.3	16.4	16.6
Pr	2.40	1.06	1.94	2.15	2.11	2.36
Nd	11.1	3.95	6.96	9.03	8.36	10.6
Sm	2.62	0.84	1.27	1.86	1.45	2.34
Eu	0.85	0.24	0.36	0.56	0.43	0.77
Gd	2.19	0.92	1.10	1.61	1.24	1.98
Tb	0.30	0.16	0.19	0.24	0.20	0.28
Dy	1.71	1.02	1.31	1.59	1.38	1.66
Y	11.3	6.76	8.66	9.93	8.99	10.7
Ho	0.35	0.22	0.29	0.33	0.31	0.36
Er	0.95	0.61	0.81	0.87	0.83	0.92
Tm	0.14	0.08	0.11	0.12	0.12	0.13
Yb	0.87	0.49	0.75	0.79	0.78	0.82
Lu	0.14	0.07	0.10	0.13	0.11	0.12
Hf	0.26	0.06	0.06	0.08	0.13	0.22
Ta	0.02	0	0	0	0	0.01
Pb	0.57	0.69	0.64	0.46	0.62	0.51
Th	0.35	0.05	0.14	0.22	0.19	0.3
U	1.07	0.08	0.14	0.69	0.32	0.98
ΣREE + Y	60.8	29.2	49.8	54.2	52.5	59.1
Y/Ho	32	31	30	30	29	30
$(La/Yb)_{SN}$	0.82	0.68	0.97	0.81	0.92	0.85
$(Ce/Ce^*)_{SN}$	0.78	0.87	0.85	0.87	0.83	0.81
$(Pr/Pr^*)_{SN}$	1.02	1.09	1.08	1.03	1.06	1.03
$(Eu/Eu^*)_{SN}$	1.77	1.31	1.42	1.59	1.53	1.77

Total Fe reported as Fe_2O_3. $(Pr/Pr^*)_{SN} = [2Pr/(Ce + Nd)]_{SN}$; $(Ce/Ce^*)_{SN} = [2Ce/(La + Pr)]_{SN}$; $(Eu/Eu^*)_{SN} = [Eu/(0.67Sm + 0.33 Tb)]_{SN}$.

surprisingly comparable with our extrapolated $\varepsilon_{Nd}(t)$ value (+3.5) of the iron-rich end member. Therefore, an $\varepsilon_{Nd}(t)$ value of +3.5 can reasonably be assigned to mid-ocean hydrothermal sources at ~2.3 Ga.

It is more difficult to precisely constrain the $\varepsilon_{Nd}(t)$ value of the continent-like end-member. Excluding low-Al meta-pelites, epiclastic meta-sediments intercalated with the Yuanjiacun BIF show geochemical features similar to those of a chemically evolved landmass consisting predominantly of felsic igneous rocks (Wang et al., 2015b). It appears plausible that surface waters (at least in the depositional basin of the BIF) could have been chemically dominated by weathering input from this landmass (e.g., Bau and Dulski, 1996; Frei and Polat, 2007; Alexander et al., 2008). The low-Al meta-pelites are highly ferruginous, reflecting dilution with BIF-type precipitates, and are thus unlikely to be representative of the composition of contemporaneous terrigenous sediments. The $\varepsilon_{Nd}(t)$ values of other clastic sediments, ranging from −0.5 to −4.3, are less radiogenic than those of the BIF, but the Nd model ages (average of ~2.8 Ga) are compatible with that of the chemical sediments (Wang et al., 2015b). Hence, it appears that the average $\varepsilon_{Nd}(t)$ value around −2.4 characterized fine-grained terrigenous epiclastic sediments during the deposition of the BIF. This value is in excellent accord with the predicted $\varepsilon_{Nd}(t)$ value above for the silica-rich source, which therefore represents the Nd isotopic composition of ambient seawater.

Using these two end-member compositions, an estimate of the mantle-derived mass fraction of Nd assuming simple binary mixing between riverine (and/or aeolian) and hydrothermal fluxes suggests that between 51% and 71% of the Nd in the Yuanjiacun BIF samples must have originated from a source possessing a depleted mantle-like Nd isotopic signature. If previous models of Fe–Nd distributions in Archean BIFs are applied (Jacobsen and Pimentel-Klose, 1988a), then the Yuanjiacun BIF suggests that the mid-ocean ridge hydrothermal flux of Fe to early Paleoproterozoic seawater was significant. This seems consistent with other lines of evidence above that iron is derived predominantly from a depleted source.

In order to constrain the silica sources, Hou et al. (2014) suggested that the depleted silicon isotopes ($\delta^{30}Si < 0$) of quartz within the Yuanjiacun BIF were indicative of a hydrothermal origin. This particular conclusion appears at odds with our results favoring a scenario of two periodically interacting water mass during precipitation of the BIF, in which Si was probably derived from ambient seawater. However, an examination of the results by Hou et al. (2014) reveals some problems. First, a lack of a correlation between the extent of Eu anomaly and Fe concentrations of the BIF samples implies a continuous systematic dilution of the REEs by a component other than seafloor-vented hydrothermal fluids. The ambient seawater was likely enriched with iron and silica relative to recent seawater (Siever, 1992; Konhauser et al., 2007). Second, those authors reported a very small spread in negative $\delta^{30}Si$ values (ranging from −1.7‰ to −0.4‰), suggesting a well-mixed seawater Si reservoir. Compared with $\delta^{30}Si$ values (−2.51‰ ~ −0.51‰, $n = 165$) in other BIFs ranging in an age from 3.8 to 2.5 Ga (Jiang et al., 1993; Ding et al., 1996; André et al., 2006; Steinhoefel et al., 2009, 2010), the $\delta^{30}Si$ signatures (up to −0.4‰) in the Yuanjiacun BIF are relatively high, implying silica precipitation from a heavier Si reservoir, probably due to mixing of hydrothermal fluids with isotopically heavier seawater. Third, silicon isotope fractionation during precipitation from solution is not well constrained, but estimates for the difference between fluid and precipitates are on the order of −1.5‰ (De La Rocha et al., 1997; Ziegler et al., 2005; Basile-Doelsch, 2006; Delstanche et al., 2009). Taking this fractionation factor together with the Si isotope composition of the Yuanjiacun samples (Hou et al., 2014), silica originated from seawater with a Si isotope signature varying between −0.2‰ and 1.1‰. Generally speaking, the Si supply to the ocean by hydrothermal fluids would have carried a Si isotope signature of near-zero, whereas continental weathering delivered Si with a Si isotope signature of ~1‰ as inferred from modern sources (De La Rocha et al., 2000; Georg et al., 2006, 2009). Hence, moderately negative $\delta^{30}Si$ values within the Yuanjiacun samples more likely reflect a significant terrigenous input of silica.

5.2. Comparison with other Nd isotopic studies of BIFs

Previous studies focusing on the neodymium isotopic variations in Precambrian BIFs have shown that the Fe-rich layers have variable iron sources, ranging from submarine hydrothermal venting

Table 2
Sm–Nd isotopic data and selected major elements of the Yuanjiacun BIF and associated quartzite.

Sample	Sm (ppm)	Nd (ppm)	$^{147}Sm/^{144}Nd$	$^{143}Nd/^{144}Nd$	$\pm 2\sigma_m$	$\varepsilon_{Nd}(0)$	$\varepsilon_{Nd}(t)$ (t = 2.3 Ga)	$f_{Sm/Nd}$	T_{DM} (Ma)	$Fe_2O_3^T$ (wt%)	SiO_2(wt%)
BIF[a]											
YJC1-1	0.59	2.98	0.1200	0.511543	0.000010	−21.4	1.3	−0.39	2603	50.5	48.9
YJC1-2	0.29	1.29	0.1356	0.511742	0.000016	−17.5	0.6	−0.31	2738	43.8	55.8
YJC1-4	0.05	0.13	0.1533	0.512046	0.000015	−11.5	1.3	−0.22	2776	50.9	48.7
YJC1-5	0.04	0.13	0.1590	0.512118	0.000020	−10.1	1.0	−0.19	2865	47.5	52.0
YJC2-2	0.25	1.34	0.1108	0.511376	0.000016	−24.6	0.8	−0.44	2618	45.8	53.3
YJC2-3	0.31	1.29	0.1457	0.511924	0.000011	−13.9	1.1	−0.26	2740	47.5	51.9
YJC3-1	0.27	1.19	0.1354	0.511793	0.000019	−16.5	1.6	−0.31	2633	52.9	42.7
YJC3-2	0.21	1.06	0.1212	0.511556	0.000020	−21.1	1.2	−0.38	2616	48.2	48.0
YJC3-4	0.14	0.38	0.1695	0.512306	0.000020	−6.5	1.6	−0.14	2902	53.4	45.6
YJC4-2	0.14	0.38	0.1392	0.511828	0.000015	−15.8	1.2	−0.29	2695	50.3	44.7
WY4	0.21	0.93	0.1338	0.511735	0.000018	−17.6	1.0	−0.32	2690	46.6	51.4
WY5	0.24	1.10	0.1307	0.511730	0.000017	−17.7	1.8	−0.34	2599	54.9	44.3
Quartzite											
WYJ-1	2.42	10.1	0.1451	0.511774	0.000010	−16.9	−1.6	−0.26	3042	9.33	90.0
WYJ-2	0.78	4.05	0.1169	0.511301	0.000011	−26.1	−2.5	−0.41	2898	0.84	98.6
WYJ-3	1.15	6.93	0.1008	0.511080	0.000012	−30.4	−2.0	−0.49	2781	1.93	97.0
WYJ-4	1.91	9.00	0.1235	0.511437	0.000009	−23.4	−1.8	−0.37	2881	5.24	94.2
WYJ-5	1.57	8.29	0.1202	0.511378	0.000011	−24.6	−2.0	−0.39	2875	3.75	95.6
WYJ-6	2.27	10.6	0.1306	0.511556	0.000011	−21.1	−1.6	−0.34	2910	8.45	90.9

[a] Major oxides contents of the BIF samples from Wang et al. (2014a, 2015a); total Fe reported as Fe_2O_3.

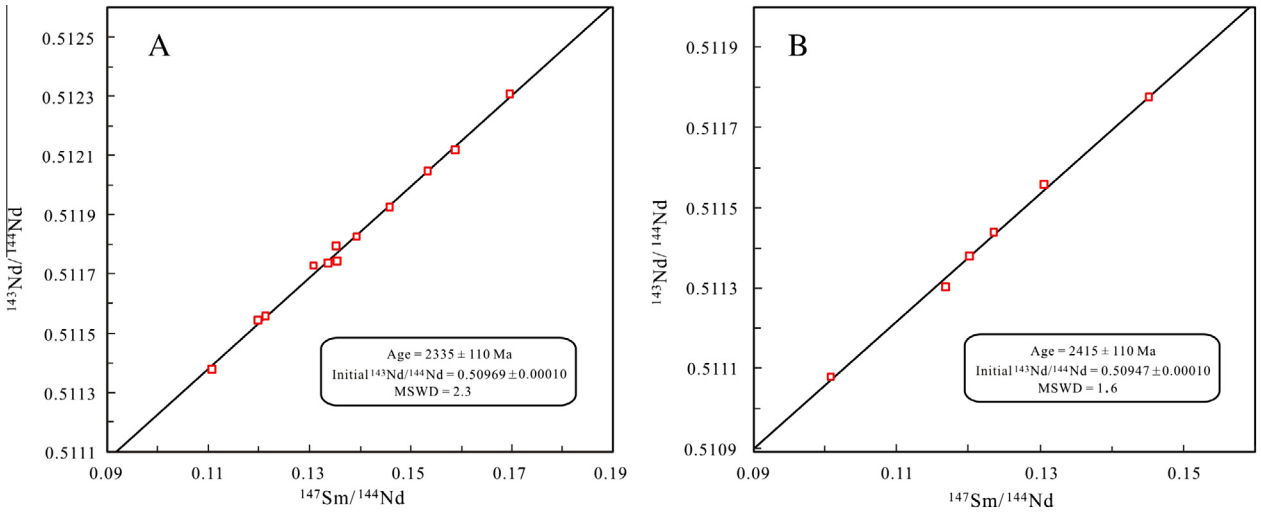

Fig. 5. Sm–Nd isochron diagram with data for the Yuanjiacun BIF (A) and intercalated quartzite (B) samples.

(e.g., Alibert and McCulloch, 1993; Bau et al., 1997; Alexander et al., 2009; Viehmann et al., 2014) to continental weathering (e.g., Alexander et al., 2008; Frei et al., 2008). Below we briefly summarize some of those studies in an attempt to show that there is in fact some inconsistency to the existing data sets.

In the ca. 2.5 Ga Hamersley Group BIFs of Western Australia, Miller and O'Nions (1985) obtained a wide range in $\varepsilon_{Nd}(t)$ values (−4.7 to +1.6), and inferred that Nd was largely supplied by continental weathering. In contrast, a similar large variation in $\varepsilon_{Nd}(t)$ values (−0.6 to +4.1) was reported by Jacobsen and Pimentel-Klose (1988a), and they interpreted this variance as reflecting regional variability in the Nd isotopic composition of authigenic components. Alibert and McCulloch (1993) reexamined the Nd isotopic data of Jacobsen and Pimentel-Klose (1988a) and argued that these initial $\varepsilon_{Nd}(t)$ values reflect a late metamorphic perturbation of the Sm–Nd system. Moreover, they reported new Nd isotopic data for 26 samples from the Hamersley (Dales Gorge and Joffre members) BIFs, concluding that these BIF samples had also suffered a metamorphic resetting of their isotopic systems some 500 Ma after deposition, a conclusion supported by Rb–Sr and Pb–Pb isotopic analyses of the underlying Fortescue lavas (Nelson et al., 1992). At the same time, initial $\varepsilon_{Nd}(t)$ values are still estimated to be +1.0 ± 0.5 at the time of deposition (~2.5 Ga), after correction for metamorphic effects. Consequently, it appears likely that the positive $\varepsilon_{Nd}(t)$ values for the Hamersley BIFs are reasonable. They are more radiogenic than those for associated shales (−0.9) (Alibert and McCulloch, 1993), suggesting that REE and iron in the BIFs were predominantly, though not exclusively, derived from hydrothermal alteration of oceanic crust.

A positive relationship between the $\varepsilon_{Nd}(t)$ and the iron content is also demonstrated for the ~3.7 Ga Isua BIF (Frei and Polat, 2007). Those authors found two distinctly positive $\varepsilon_{Nd}(t)$ values corresponding to two interacting water masses (high-T hydrothermal fluids and ambient seawater): a Fe-rich end-member (magnetite-rich bands) with $\varepsilon_{Nd}(t)$ values of ~+3.1 and a Fe-poor end-member (quartz-rich bands) with $\varepsilon_{Nd}(t)$ values of ~+1.2. Their results imply that REE of early Archean surface waters were dominated by depleted landmass sources rather than enriched continental crusts, as in our case. This is consistent with other evidence that suggest the presence of a chemically evolved crust

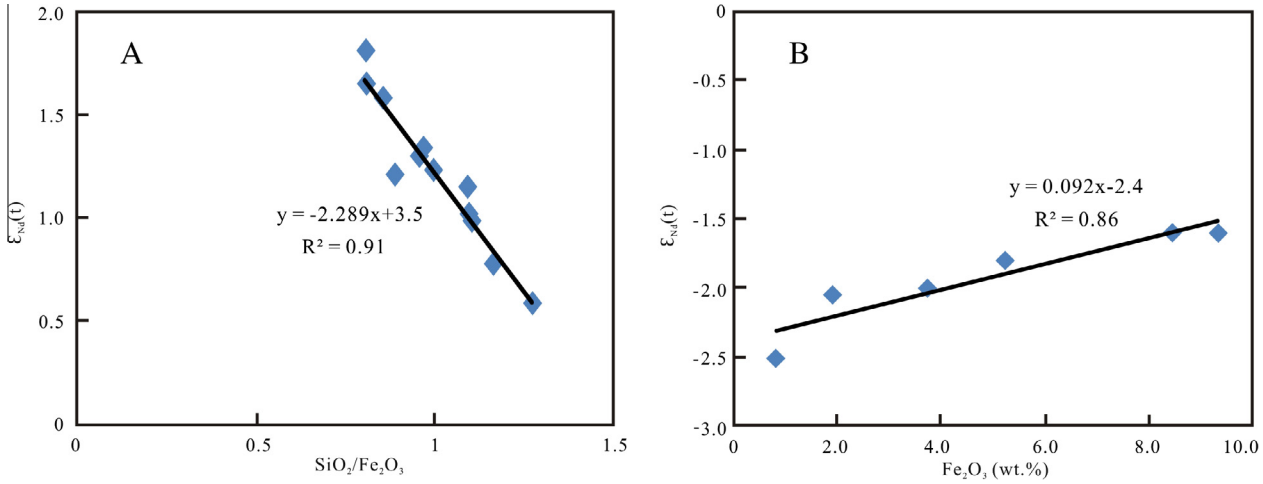

Fig. 6. (A) Diagram showing the reverse relationship between SiO_2/Fe_2O_3 ratios and $\varepsilon_{Nd}(t = 2.3\ Ga)$ values of the Yuanjiacun BIF samples. (B) Diagram showing the positive correlation between total iron (expressed as Fe_2O_3) concentrations and initial ε_{Nd} values of the ferruginous quartzite samples.

(protocrust) composed of essentially depleted rocks (e.g., a suit of garnet-mica schists with the $\varepsilon_{Nd}(t)$ value of +1.7) (Kamber et al., 1998, 2005).

However, it is worth noting that negative $\varepsilon_{Nd}(t)$ signatures have also been recorded in a few cases (e.g., Alibert and McCulloch, 1993; Alexander et al., 2008; Frei et al., 2008; Døssing et al., 2009; Haugaard et al., 2013; Wang et al., 2014c). This continental-type Nd may be due to (i) higher riverine REE input derived from weathering of locally exposed enriched continental crust, or (ii) additional REE input from submarine hydrothermal fluids interacted with terrigenous clastic sediments covering oceanic spreading centers or an underlying enriched continental crust, or (iii) significant REE input from seafloor-vented hydrothermal fluids derived from interaction with a locally enriched mantle source. For instance, the ~2.6 Ga Marra Mamba BIF in western Australia and associated rocks (Jeerinah shales/cherts, Wittenoom Dolomite and McRae Shale units) have a similar average $\varepsilon_{Nd}(t)$ value of -0.6 ± 0.9 (Alibert and McCulloch, 1993), suggesting that Nd was mostly supplied by erosional products coming from the nearby upper Fortescue Group. Modern analogs can be found in restricted basins, such as Baffin Bay, where the seawater neodymium isotopic composition is strongly influenced by the surrounding Archean terranes (Stordal and Wasserburg, 1986).

In addition, Døssing et al. (2009) have put forward another situation for the ~2.7 Ga BIFs with continental-type $\varepsilon_{Nd}(t)$ values from the Tati greenstone belt (TGB) in the northeast of Botswana. In their study, there exists a negative relationship between Fe_2O_3 and Sm–Nd isotopes of the TGB BIFs. The iron-rich source is associated with a source that is significantly enriched ($\varepsilon_{Nd}(t) = -2.5$) relative to the Si-rich source ($\varepsilon_{Nd}(t) = -0.4$). Combining the negative $\varepsilon_{Nd}(t)$ values measured for associated volcanic rocks (average of −1.3) and the less negative $\varepsilon_{Nd}(t)$ values defined by sedimentary rocks (average of −0.4), they proposed that mixing of two different sources best explained the features of the TGB BIFs, namely seafloor-vented hydrothermal fluids that received their Sm–Nd isotopic signature from enriched mantle lithospheric materials, and ambient surface basin waters whose REE signature was controlled by solutes derived from weathering of nearby enriched continental landmasses. Such mantle enrichment, potentially by ancient recycling of continentally derived material into the mantle, is generally compatible with other lines of evidence (e.g., Re–Os isotopic features of chromite-bearing layered intrusions, Nägler et al., 1997).

Recently, negative $\varepsilon_{Nd}(t)$ features were also found in the ~2.9 Ga Itilliarsuk BIF in the West Greenland (Haugaard et al., 2013). Surprisingly, these subchondritic values are only found for the Al-poor (<0.5 wt%) and iron-rich bands. Additionally, the associated supracrustal rocks, consisting of shales, greywackes, and acidic metavolcanics, have significantly positive $\varepsilon_{Nd}(t)$ values. In this regard, submarine hydrothermal fluids sourced from an older, but now unexposed, enriched reservoir were responsible for the input of iron and Nd to the BIF. It is likely that terrigenous sediments covering oceanic crusts defined this unusual source in terms of the inferred juvenile ocean island arc setting for the BIF (Haugaard et al., 2013). It appears that the high-T hydrothermal input indicated by positive Eu anomalies in the BIF did not overwhelm the terrestrial flux in terms of the Nd isotope signature. Similar examples of the lack of correlation between mantle-like Nd isotopic signatures and positive Eu anomalies in high-T hydrothermal fluids have been found in modern submarine hydrothermal systems (Piepgras and Wasserburg, 1985; Klinkhammer et al., 1994; German et al., 1995). For example, Piepgras and Wasserburg (1985) reported Nd isotopic data for a hydrothermal system developed on a sediment-covered ridge in the Guaymas Basin, Gulf of California. The vented hydrothermal fluid ($T > 300\ °C$) migrated through a sedimentary package several hundred meters thick. In contrast to solutions from sediment-starved ridges, which show positive Eu anomalies and positive $\varepsilon_{Nd}(t)$ values (Klinkhammer et al., 1994), this solution possesses similar Eu anomalies but displays negative $\varepsilon_{Nd}(t)$ values ($\varepsilon_{Nd}(0) = -11.4$), indicating that the Nd isotopic signatures of marine fluids are controlled by compositions of host rocks (Alexander et al., 2008). In addition, similar explanations can be also utilized to account for the Sm–Nd isotopic data of the 2.5 Ga Wangjiazhuang BIF in China (Wang et al., 2014c). The only difference is that, considering a continental marginal arc setting for the basin where the BIF was precipitated, an interaction of hydrothermal fluids with underlying older enriched continental crusts is responsible for the observed continent-type Nd isotopic compositions.

5.3. Nd isotopic variations throughout the Archean and Paleoproterozoic ocean

Seawater Nd compositions are controlled predominantly by source compositions of which two potential end-members are run-off from continental crust and depleted mantle input from submarine hydrothermal systems (Bolhar et al., 2002). The isotopic composition of Nd in marine chemical precipitates, such as BIFs, may place better constraints on the relative magnitude of these two influxes. Generally, BIFs older than 1.84 Ga have $\varepsilon_{Nd}(t)$ values

between −5 and +5 (Fig. 7), with much of the data describing the Archean BIFs. Many BIFs, with ages of 3.7 to 2.3 Ga, have predominantly positive $\varepsilon_{Nd}(t)$ values, suggesting that hydrothermal alteration of oceanic crust dominates the Nd (and hence Fe?) flux to ancient seawater. Certainly more studies on Mesoarchean (3.5–3.0 Ga) and mid-Paleoproterozoic (2.3–2.0 Ga) units are necessary, but existing Nd isotopic data are consistent with the increased mantle-derived hydrothermal flux as evidenced by higher Mn and Ba concentrations and low mantle-like Sr isotopic ratios in Archean marine carbonates (Fryer et al., 1979; Veizer et al., 1982; Eglington et al., 2003; Kamber and Webb, 2001). The higher mantle contribution to the Archean oceans is consistent with models of higher heat production (McKenzie and Weiss, 1975) and higher sea-floor production rates (Abbott and Hoffman, 1984) during the Archean. Nevertheless, from Archean to Proterozoic, there is a gradual decrease in hydrothermal activities as the Earth cooled (Fryer, 1977; Condie, 1997; Arndt et al., 2008). Evidence for this comes from the general trend of decreasing positive Eu anomalies with decreasing age of BIFs (Frei et al., 2008; Haugaard et al., 2013) and a progressive decrease in Ni concentration through time in BIFs (Pecoits et al., 2009; Konhauser et al., 2009). The latter can also be explained as a result of a compositional change from an ultramafic to a more felsic upper continental crust (Condie, 1993), which is most likely a direct consequence of cooling of the mantle with time (Arndt, 1991; Berry et al., 2008). Moreover, the diminishing hydrothermal input is likely to be exemplified by the late Paleoproterozoic BIFs (~1.9 Ga) on disparate cratonic margins (e.g., Superior), which have variable but mostly negative $\varepsilon_{Nd}(t)$ values, indistinguishable in this respect from their contemporary fine-grained clastic sediments (Miller and O'Nions, 1985; Jacobsen and Pimentel-Klose, 1988b). Collectively, these results reflect a stronger continental contribution of Nd to the ocean. In addition, tidal signatures (Chandler, 1984) and identical depositional ages (Rasmussen et al., 2012) for these BIFs support arguments that their deposition is likely to reflect the chemistry of the global ocean rather than restricted basin-scale conditions.

Data for BIFs older than 2.3 Ga are sometimes dominated by studies of a few samples with negative $\varepsilon_{Nd}(t)$ values (Fig. 7). They are primarily dependent upon the nature of local mantle or continental crust exposed to weathering or unexposed for hydrothermal leaching, which have been described in detail above. However, these enriched $\varepsilon_{Nd}(t)$ records for the BIFs are not entirely unusual, as supported by recent investigations of Archean shallow carbonates from southern Africa (Bolhar et al., 2002; Kamber et al., 2004). These studies concluded that the site of carbonate precipitation may have been a basin which was proximal to continental crust, since negative $\varepsilon_{Nd}(t)$ values and REY features indicate a strong continental influence and no indication of mantle-derived REE as might be expected in a distant oceanic environment. These enriched signatures are in marked contrast to Nd compositions obtained for other BIFs with positive values (Appendix Table) requiring a seawater composition dominated by mantle input. We, therefore, interpret the discrepancy as indicating that ancient seawater (>2.3 Ga) was temporally and spatially heterogeneous with respect to $^{143}Nd/^{144}Nd$ ratios. Even in the one same basin, the source heterogeneity for the BIF and syn-depositional sediments is also observed. For instance, our study can be used to characterize this short-lived fluctuation of the Nd isotopic composition of seawater. The Yuanjiacun BIF and associated meta-chert (quartzite) samples display clearly distinct $\varepsilon_{Nd}(t)$ values (consistently positive and negative, respectively), suggesting various degrees of mixing of ambient seawater and high-T hydrothermal fluids.

A similarly heterogenous scenario is observed in the modern oceans. So far, there is clear evidence that hydrothermal sources only contribute ≈2.5% of the total flux of Nd supplied to the present oceans because of an immediate immobilization or scavenging of Nd by hydrothermal precipitates very close to or even within the hydrothermal sources (Goldstein and Jacobsen, 1987; German et al., 1990). Riverine input, particularly in regimes of strong chemical weathering, is a very important source (more than 90%) for the dissolved Nd budget of water masses, although most of the dissolved Nd load of rivers is precipitated in the estuarine sediments (Elderfield et al., 1990; Ingri et al., 2000). As a consequence, the Nd isotopic signatures for a particular water mass are closely related to the riverine Nd input derived from weathering of different types and ages of nearby continental crusts (Stordal and Wasserburg, 1986; Bertram and Elderfield, 1993; Amakawa et al., 2000). Generally, modern seawater possesses negative $\varepsilon_{Nd}(0)$ values between 0 and −20 (Frank, 2002) with some extreme values restricted to shallow waters (Stordal and Wasserburg, 1986). The water column of the world ocean is also quite spatially inhomogenous in $\varepsilon_{Nd}(0)$ owing to inefficient vertical and horizontal mixing of marine water

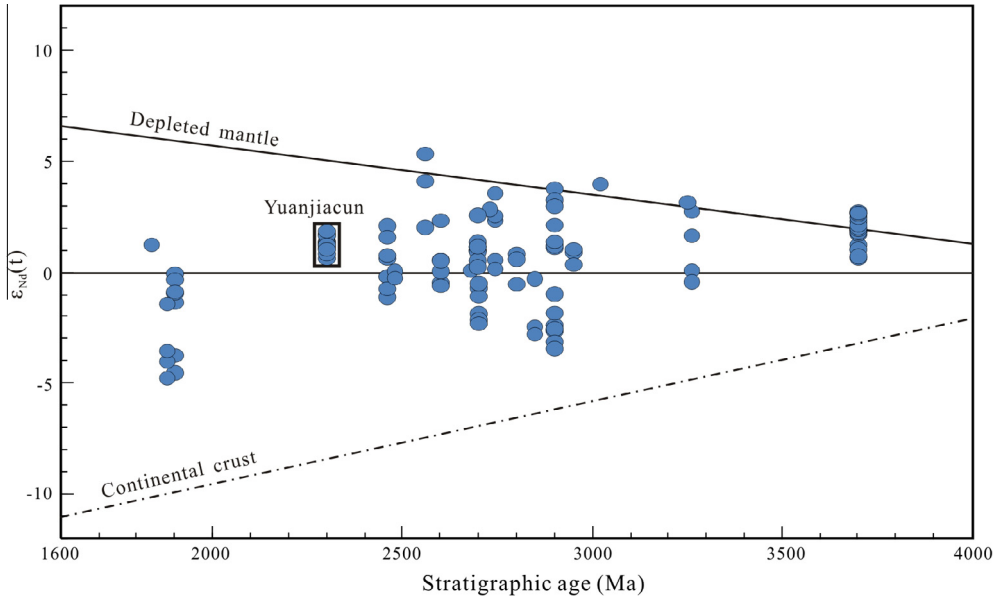

Fig. 7. Neodymium isotopic signatures of the Archean and Paleoproterozoic BIFs older than 1.8 Ga. Data are screened to distinguish reliable samples which represent the best archives of coeval Precambrian seawater $^{143}Nd/^{144}Nd$. Detailed $\varepsilon_{Nd}(t)$ and age data and relevant references are presented in Appendix Table.

in some local basins (Piepgras and Wasserburg, 1982; Jeandel, 1993; Shimizu et al., 1994; Jeandel et al., 1995, 1998). Temporal variability in seawater $\varepsilon_{Nd}(t)$ has also been noted. For example, Recent (<20 Ka) seawater Nd ratios appear to have fluctuated by 2–3 ε_{Nd}-units on 1000–5000 yr time scales (e.g., Abouchami et al., 1997; Gutjahr et al., 2008).

6. Conclusions

All of the selected 2.3–2.2 Ga Yuanjiacun BIF and interbedded meta-chert samples show characteristic features resembling those of other BIFs worldwide, including PAAS-normalized LREE depleted REE + Y patterns relative to HREE, positive La and Eu anomalies, and superchondritic Y/Ho ratios. With the exception of Eu and Ce anomalies, these are typical features of modern seawater. Positive Eu anomalies indicate a high-T hydrothermal source supplied REEs to the seawater from which the BIF precipitated.

Sm–Nd isotopic data and corresponding correlations between Nd isotopes and major components of the BIF and meta-chert samples allow for a further characterization of the two interacting water masses (ambient surface seawater and seafloor-vented hydrothermal fluids). The former is characterized by negative $\varepsilon_{Nd}(t)$ values (inferred end-member $\varepsilon_{Nd}(t) = -2.4$), similar to the one defined by spatially associated clastic meta-sediments, and is associated with high Si fluxes. The REE contents were controlled by solutes derived from weathering of nearby continental landmasses. The latter is characterized by positive $\varepsilon_{Nd}(t)$ values (inferred end-member $\varepsilon_{Nd}(t) = +3.5$) and is associated with high-Fe fluxes. The Sm–Nd isotopic feature was sourced from hydrothermal alteration of depleted oceanic crustal rocks. The Nd isotopic mass balance calculations of the Yuanjiacun BIF indicate that most (>50%) of the Nd and iron were derived from hydrothermal sources related to mid-ocean ridge volcanism.

Taking other reported Nd isotopic data of the Archean and Paleoproterozoic BIFs together, the Nd isotopic evolution of the coeval Precambrian seawater is obtained. It is concluded that the great majority of Nd in bulk seawater prior to 2.3 Ga originated from the hydrothermal circulation through depleted mantle-derived mafic source rocks rather than sedimentary continental source material transported by river water. However, negative and continent-like $\varepsilon_{Nd}(t)$ values recorded in some BIFs argue against a mid-ocean ridge hydrothermal system as the dominant REY source, thus reflecting spatial and temporal heterogeneity with respect to the Nd isotopic composition in Earth's early oceans, as is the case today in the modern oceans.

Acknowledgments

This research was financially supported by the Major State Basic Research Programme of the People's Republic of China (No. 2012CB416601), the China Postdoctoral Science Foundation and the National Natural Science Foundation of China (No. 41372100). We would like to thank Zhuyin Chu, Chaofeng Li, Yan Yan, Yanpei Dai for their help in Sm–Nd analyses. We also would like to thank editor Guochun Zhao and three anonymous reviewers for providing detailed and insightful review comments.

Appendix A. Supplementary data

Appendix Table Sm–Nd isotopic data of the selected Archean and Paleoproterozoic BIFs.

Supplementary data associated with this article can be found, in the online version, at http://dx.doi.org/10.1016/j.precamres.2016.04.016.

References

Abbott, D.H., Hoffman, S.E., 1984. Archaean plate tectonics revisited 1. Heat flow, spreading rate, and the age of subducting oceanic lithosphere and their effects on the origin and evolution of continents. Tectonics 3, 429–448.
Abouchami, W., Goldstein, S.L., Galer, S.J.G., Eisenhauer, A., Mangini, A., 1997. Secular changes of lead and neodymium in central Pacific seawater recorded by a Fe–Mn crust. Geochim. Cosmochim. Acta 61, 3957–3974.
Alexander, B.W., Bau, M., Andersson, P., Dulski, P., 2008. Continentally-derived solutes in shallow Archean seawater: rare earth element and Nd isotope evidence in iron formation from the 2.9 Ga Pongola Supergroup, South Africa. Geochim. Cosmochim. Acta 72, 378–394.
Alexander, B.W., Bau, M., Andersson, P., 2009. Neodymium isotopes in Archean seawater and implications for the marine Nd cycle in Earth's early oceans. Earth Planet. Sci. Lett. 283, 144–155.
Alibert, C., McCulloch, M.T., 1993. Rare earth element and Nd isotopic compositions of the banded iron-formations and associated shales from Hamersley, Western Australia. Geochim. Cosmochim. Acta 57, 187–204.
Amakawa, H., Alibo, D.S., Nozaki, Y., 2000. Nd isotopic composition and REE pattern in the surface waters of the eastern Indian Ocean and its adjacent seas. Geochim. Cosmochim. Acta 64, 1715–1727.
André, L., Cardinal, D., Alleman, L.Y., Moorbath, S., 2006. Silicon isotopes in 3.8 Ga West Greenland rocks as clues to the Eoarchaean supracrustal Si cycle. Earth Planet. Sci. Lett. 245, 162–173.
Arndt, N.T., 1991. High Ni in Archean tholeiites. Tectonophysics 187, 411–420.
Arndt, N.T., Barnes, S.J., Lesher, C.M., 2008. Komatiite. Cambridge University Press, p. 488.
Basile-Doelsch, I., 2006. Si stable isotopes in the Earth's surface: a review. J. Geochem. Explor. 88, 252–256.
Bau, M., 1993. Effects of syn- and post-depositional processes on the rare-earth element distribution in Precambrian Iron-formations. Eur. J. Mineral. 5, 257–267.
Bau, M., Alexander, B., 2006. Preservation of primary REE patterns without Ce anomaly during dolomitization of Mid-Paleoproterozoic limestone and the potential reestablishment of marine anoxia immediately after the "Great Oxidation Event". S. Afr. J. Geol. 109, 81–86.
Bau, M., Dulski, P., 1996. Distribution of yttrium and rare-earth elements in the Penge and Kuruman iron-formations, Transvaal Supergroup, South Africa. Precambrian Res. 79, 37–55.
Bau, M., Dulski, P., 1999. Comparing yttrium and rare-earth in hydrothermal fluids from the Mid-Atlantic Ridge: implications for Y and REE behaviour during near vent mixing and for the Y/Ho ratio of Proterozoic seawater. Chem. Geol. 155, 77–90.
Bau, M., Höhndorf, A., Dulski, P., Beukes, N.J., 1997. Sources of rare-earth elements and iron in Paleoproterozoic iron formations from the Transvaal Supergroup, South Africa: evidence from neodymium isotopes. J. Geol. 105, 121–129.
Bekker, A., Slack, J.F., Planavsky, N., Krapež, B., Hofmann, A., Konhauser, K.O., Rouxel, O.J., 2010. Iron formation: the sedimentary product of a complex interplay among mantle, tectonic, oceanic, and biospheric processes. Econ. Geol. 105, 467–508.
Berry, J.A., Danyushevsky, L.V., O'Neil, H.S.t.C., Newville, M., Sutton, S.R., 2008. Oxidation state of iron in komatiitic melt inclusions indicates hot Archean mantle. Nature 455, 960–963.
Bertram, C.J., Elderfield, H., 1993. The geochemical balance of the rare earth elements and neodymium isotopes in the oceans. Geochim. Cosmochim. Acta 57, 1957–1986.
Bolhar, R., Hofmann, A., Woodhead, J., Hergt, J., Dirks, P., 2002. Pb and Nd-isotope systematics of stromatolitic limestones from the 2.7 Ga Ngezi Group of the Belingwe Greenstone Belt: constraints on timing of deposition and provenance. Precambrian Res. 114, 277–294.
Bolhar, R., Kamber, B.S., Moorbath, S., Fedo, C.M., Whitehouse, M.J., 2004. Characterisation of early Archaean chemical sediments by trace element signatures. Earth Planet. Sci. Lett. 222, 43–60.
Chandler, F.W., 1984. Metallogenesis of an Early Proterozoic foreland sequence, eastern Hudson Bay, Canada. J. Geol. Soc. 141, 299–313.
Chu, Z.Y., Wu, F.Y., Walker, R.J., Rudnick, R.L., Pitcher, L., Puchtel, I.S., Yang, Y.H., Wilde, S.A., 2009. Temporal evolution of the lithospheric mantle beneath the eastern North China Craton. J. Petrol. 50, 1857–1898.
Condie, K.C., 1993. Chemical composition and evolution of the upper continental crust: contrasting results from surface samples and shales. Chem. Geol. 104, 1–37.
Condie, K.C., 1997. Plate Tectonics and Crustal Evolution. Butterworth-Heinemann, Oxford, p. 282.
De La Rocha, C.L., Brzezinski, M.A., DeNiro, M.J., 1997. Fractionation of silicon isotopes by marine diatoms during biogenic silica formation. Geochim. Cosmochim. Acta 61, 5051–5056.
De La Rocha, C.L., Brzezinski, M.A., DeNiro, M.J., 2000. A first look at the distribution of the stable isotopes of silicon in natural waters. Geochim. Cosmochim. Acta 64, 2467–2477.
Delstanche, S., Opfergelt, S., Cardinal, D., Elsass, F., André, L., Delvaux, B., 2009. Silicon isotopic fractionation during adsorption of aqueous monosilicic acid onto iron oxide. Geochim. Cosmochim. Acta 73, 923–934.
DePaolo, D.J., 1981. Neodymium isotopes in the Colorado Front Range and crust-mantle evolution in the Proterozoic. Nature 291, 193–196.

Derry, L.A., Jacobsen, S.B., 1990. The chemical evolution of Precambrian seawater: evidence from REEs in banded iron formations. Geochim. Cosmochim. Acta 54, 2965–2977.
Ding, T., Jiang, S., Wang, D., 1996. Silicon Isotope Geochemistry. Geological Publishing House, Beijing.
Døssing, L.N., Frei, R., Stendal, H., Mapeo, R.B.M., 2009. Characterization of enriched lithospheric mantle components in ~2.7 Ga banded iron formations: an example from the Tati Greenstone Belt, Northeastern Botswana. Precambrian Res. 172, 334–356.
Dymek, R.F., Klein, C., 1988. Chemistry, petrology, and origin of banded iron-formation lithologies from the 3800 Ma Isua Supracrustal Belt, West Greenland. Precambrian Res. 39, 247–302.
Eglington, B.M., Talma, A.S., Marais, S., Matthews, P.E., Dixon, J.G.P., 2003. Isotopic composition of Pongola Supergroup limestones from the Buffalo River gorge, South Africa: constraints on their regional depositional setting. S. Afr. J. Geol. 106, 1–10.
Elderfield, H., Upstill-Goddard, R., Sholkovitz, E.R., 1990. The rare earth elements in rivers, estuaries, and coastal seas and their significance to the composition of ocean waters. Geochim. Cosmochim. Acta 54, 971–991.
Frank, M., 2002. Radiogenic isotopes: tracers of past ocean circulation and erosional input. Rev. Geophys. 40, 1–38.
Frei, R., Polat, A., 2007. Source heterogeneity for the major components of ~3.7 Ga banded iron formations (Isua Greenstone Belt, Western Greenland): tracing the nature of interacting water masses in BIF formation. Earth Planet. Sci. Lett. 253, 266–281.
Frei, R., Dahl, P.S., Duke, E.F., Frei, K.M., Hansen, T.R., Frandsson, M.M., Jensen, L.A., 2008. Trace element and isotopic characterization of Neoarchean and Paleoproterozoic iron formations in the Black Hills (South Dakota, USA): assessment of chemical change during 2.9–1.9 Ga deposition bracketing the 2.4–2.2 Ga first rise of atmospheric oxygen. Precambrian Res. 162, 441–474.
Fryer, B.J., 1977. Rare earth evidence in iron formations for changing Precambrian oxidation states. Geochim. Cosmochim. Acta 41, 361–367.
Fryer, B.J., Fyfe, W.S., Kerrich, R., 1979. Archaean volcanogenic oceans. Chem. Geol. 24, 25–33.
Geng, Y.S., Wan, Y.S., Shen, Q.H., Li, H.M., Zhang, R.X., 2000. Chronological framework of the Early Precambrian important events in the Lüliang Area, Shanxi Province. Acta Petrol. Sin. 74, 216–223.
Geng, Y.S., Yang, C.H., Song, B., Wan, Y.S., 2004. Post-orogenic granites with an age of 1800 Ma in Lüliang area, North China Craton: constraints from isotopic geochronology and geochemistry. Geol. J. Chin. Univ. 10, 477–487.
Geng, Y.S., Wan, Y.S., Yang, C.H., 2008. The Set of Main Geological Events in the Paleoproterozoic Lüliang Area, Shanxi Province. Geological Publishing House, Beijing, pp. 515–533.
Georg, R.B., Reynolds, B.C., Frank, M., Halliday, A.N., 2006. Mechanisms controlling the silicon isotopic composition of river waters. Earth Planet. Sci. Lett. 249, 290–306.
Georg, R.B., West, A.J., Basu, A.R., Halliday, A.N., 2009. Silicon fluxes and isotope composition of direct groundwater discharge into the Bay of Bengal and the effect on the global ocean silicon isotope budget. Earth Planet. Sci. Lett. 283, 67–74.
German, C.R., Klinkhammer, G.P., Edmond, J.M., Mitra, A., Elderfield, H., 1990. Hydrothermal scavenging of rare-earth elements in the ocean. Nature 345, 516–518.
German, C.R., Barreiro, B.A., Higgs, N.C., Nelson, T.A., Ludford, E.M., Palmer, M.R., 1995. Seawater-metasomatism in hydrothermal sediments (Esca-naba Trough, northeast Pacific). Chem. Geol. 119, 175–190.
Goldstein, S.J., Jacobsen, S.B., 1987. The Nd and Sr isotopic systematics of river water dissolved material: implications for the sources of Nd and Sr in seawater. Chem. Geol. 66, 245–272.
Gutjahr, M., Frank, M., Stirling, C.H., Keigwin, L.D., Halliday, A.N., 2008. Tracing the Nd isotope evolution of North Atlantic Deep and intermediate waters in the western North Atlantic since the Last Glacial Maximum from Blake Ridge sediments. Earth Planet. Sci. Lett. 266, 61–77.
Haugaard, R., Frei, R., Stendal, H., Konhauser, K.O., 2013. Petrology and geochemistry of the ~2.9 Ga Itilliarsuk banded iron formation and associated supracrustal rocks, West Greenland: Source characteristics and depositional environment. Precambrian Res. 229, 150–176.
Holland, H.H., 1984. The Chemical Evolution of the Atmosphere and the Oceans. Princeton University Press.
Hou, K., Li, Y., Gao, J., Liu, F., Qin, Y., 2014. Geochemistry and Si–O–Fe isotope constraints on the origin of banded iron formations of the Yuanjiacun Formation, Lvliang Group, Shanxi, China. Ore Geol. Rev. 57, 288–298.
Ingri, J., Widerlund, A., Land, M., Gustafsson, Ö., Andersson, P., Öhlander, B., 2000. Temporal variations in the fraction of the rare earth elements in a boreal river: the role of colloidal particles. Chem. Geol. 166, 23–45.
Isley, A.E., Abbott, D.H., 1999. Plume-related mafic volcanism and the deposition of banded iron formation. J. Geophys. Res. 104, 15461–15477.
Jacobsen, S.B., Pimentel-Klose, M.R., 1988a. A Nd isotopic study of the Hamersley and Michipicoten banded iron formations: the source of REE and Fe in Archean oceans. Earth Planet. Sci. Lett. 87, 29–44.
Jacobsen, S.B., Pimentel-Klose, M.R., 1988b. Nd isotopic variations in Precambrian banded iron formations. Geophys. Res. Lett. 15, 393–396.
Jeandel, C., 1993. Concentration and isotopic composition of Nd in the Southern Atlantic Ocean. Earth Planet. Sci. Lett. 117, 581–591.
Jeandel, C., Bishop, J.K., Zindler, A., 1995. Exchange of neodymium and its isotopes between seawater and small and large particles in the Sargasso Sea. Geochim. Cosmochim. Acta 59, 535–547.
Jeandel, C., Thouron, D., Fieux, M., 1998. Concentrations and isotopic compositions of neodymium in the eastern Indian Ocean and Indonesian Straits. Geochim. Cosmochim. Acta 62, 2597–2607.
Jiang, S.Y., Ding, T.P., Wan, D.F., Li, Y.H., 1993. Silicon isotopic compositions of Archean banded Si–Fe formation (BIF) in the Gongchangling ore deposit, Liaoning-Province, China. Sci. Chin. 36 (Series B), 482–489, Chemistry.
Kamber, B.S., Webb, G.E., 2001. The geochemistry of late Archaean microbial carbonate: implications for ocean chemistry and continental erosion history. Geochim. Cosmochim. Acta 65, 2509–2525.
Kamber, B.S., Moorbath, S., Whitehouse, M.J., 1998. Extreme Nd isotope heterogeneity in the early Archean-fact or fiction? Case histories from northern Canada and West Greenland-reply. Chem. Geol. 148, 219–224.
Kamber, B.S., Bohlar, R., Webb, G.E., 2004. Geochemistry of late Archaean stromatolites from Zimbabwe: evidence for microbial life in restricted epicontinental seas. Precambrian Res. 132, 379–399.
Kamber, B.S., Whitehouse, M.J., Bolhar, R., Moorbath, S., 2005. Volcanic resurfacing and the early terrestrial crust: zircon U–Pb and REE constraints from the Isua Greenstone Belt, southern West Greenland. Earth Planet. Sci. Lett. 240, 276–290.
Klein, C., 2005. Some Precambrian banded iron-formations (BIFs) from around the world: their age, geologic setting, mineralogy, metamorphism, geochemistry, and origins. Am. Mineral. 90, 1473–1499.
Klinkhammer, G.P., Elderfield, H., Edmond, J.M., Mitra, A., 1994. Geochemical implications of rare-earth element patterns in hydrothermal fluids from mid-ocean ridges. Geochim. Cosmochim. Acta 58, 5105–5113.
Konhauser, K.O., Amskold, L., Lalonde, S.V., Posth, N.R., Kappler, A., Anbar, A., 2007. Decoupling photochemical Fe(II) oxidation from shallow-water BIF deposition. Earth Planet. Sci. Lett. 258, 87–100.
Konhauser, K.O., Pecoits, E., Lalonde, S.V., Papineau, D., Nisbet, E.G., Barley, M.E., Arndt, N.T., Zahnle, K., Kamber, B.S., 2009. Oceanic nickel depletion and a methanogen famine before the great oxidation event. Nature 458, 750–753.
Liu, S.W., Li, Q.G., Liu, C.H., Lü, Y.J., Zhang, F., 2009. Guandishan granitoids of the Paleoproterozoic Lüliang metamorphic complex in the Trans-North China Orogen: SHRIMP zircon ages, petrogenesis and tectonic implications. Acta Geol. Sin. 83, 580–602 (English edition).
Liu, S.W., Zhang, J., Li, Q.G., Zhang, L.F., Wang, W., Yang, P.T., 2012. Geochemistry and U–Pb zircon ages of metamorphic volcanic rocks of the Paleoproterozoic Lüliang Complex and constraints on the evolution of the Trans-North China Orogen, North China Craton. Precambrian Res. 222, 173–190.
Liu, C.H., Zhao, G.C., Liu, F.L., Shi, J.R., 2014. Geochronological and geochemical constraints on the Lüliang Group in the Lüliang Complex: implications for the tectonic evolution of the Trans-North China Orogen. Lithos 198, 298–315.
McKenzie, D., Weiss, N., 1975. Speculations on the thermal and tectonic history of the Earth. Geophys. J. R. Astron. Soc. 42, 131–174.
McLennan, S.M., 1989. Rare earth elements in sedimentary rocks: influence of provenance and sedimentary processes. In: Lipin, B.R., McKay, G.A. (Eds.), Geochemistry and Mineralogy of Rare Earth Elements, Rev. Miner. Mineralogical Society of America, 21, pp. 169–200.
Miller, R.G., O'Nions, R.K., 1985. Sources of Precambrian chemical and clastic sediments. Nature 314, 325–330.
Mloszewska, A.M., Pecoits, E., Cates, N.L., Mojzsis, S.J., O'Neil, J., Robbins, L.J., Konhauser, K.O., 2012. The composition of Earth's oldest iron formations: the Nuvvuagittuq Supracrustal Belt (Québec, Canada). Earth Planet. Sci. Lett. 317, 331–342.
Mloszewska, A.M., Mojzsis, S.J., Pecoits, E., Papineau, D., Dauphas, N., Konhauser, K. O., 2013. Chemical sedimentary protoliths in the >3.75 Ga Nuvvuagittuq Supracrustal Belt (Québec, Canada). Gondwana Res. 23 (2), 574–594.
Nägler, T.F., Kramers, J.D., 1998. Nd isotopic evolution of the upper mantle during the Precambrian: Models, data and the uncertainty of both. Precambrian Res. 91, 233–252.
Nägler, T.F., Kramers, J.D., Kamber, B.S., Frei, R., Prendergast, M.D.A., 1997. Growth of subcontinental lithospheric mantle beneath Zimbabwe started at or before 3.8 Ga: Re–Os study on chromites. Geology 25, 983–986.
Nelson, D.R., Trendall, A.F., De Laeter, J.R., Grobler, N.J., Fletcher, I.R., 1992. A comparative study of the geochemical and isotopic systematics of late Archean flood basalts from the Pilbara and Kaapvaal Cratons. Precambrian Res. 54, 231–256.
Pecoits, E., Gingras, M.K., Barley, M.E., Kappler, A., Posth, N.R., Konhauser, K.O., 2009. Petrography and geochemistry of the Dales Gorge banded iron formation: paragenetic sequence, source and implications for palaeo-ocean chemistry. Precambrian Res. 172, 163–187.
Piepgras, D.J., Wasserburg, G.J., 1982. Isotopic composition of neodymium in waters from the Drake Passage. Science 217, 207–214.
Piepgras, D.J., Wasserburg, G.J., 1985. Strontium and neodymium isotopes in hot springs on the East Pacific Rise and Guaymas Basin. Earth Planet. Sci. Lett. 72, 341–356.
Planavsky, N., Bekker, A., Rouxel, O.J., Kamber, B.S., Hofmann, A.W., Knudsen, A., Lyons, T.W., 2010. Rare earth element and yttrium compositions of Archean and Paleoproterozoic Fe formations revisited: new perspectives on the significance and mechanisms of deposition. Geochim. Cosmochim. Acta 74, 6387–6405.
Rasmussen, B., Fletcher, I.R., Bekker, A., Muhling, J.R., Gregory, C.J., Thorne, A.M., 2012. Deposition of 1.88-billion-year-old iron formations as a consequence of rapid crustal growth. Nature 484, 498–501.

Shimizu, H., Umemoto, N., Masuda, A., Appel, P.W.U., 1990. Sources of iron-formations in the Archean Isua and Malene supracrustals, West Greenland: Evidence from La–Ce and Sm–Nd isotopic data and REE. Geochim. Cosmochim. Acta 54, 1147–1154.

Shimizu, H., Tachikawa, K., Masuda, A., Nozaki, Y., 1994. Cerium and Nd isotope ratios and REE patterns in seawater from the North Pacific ocean. Geochim. Cosmochim. Acta 58, 323–333.

Siever, R., 1992. The silica cycle in the Precambrian. Geochim. Cosmochim. Acta 56, 3265–3272.

Steinhoefel, G., Horn, I., von Blanckenburg, F., 2009. Micro-scale tracing of Fe and Si isotope signatures in banded iron formation using femtosecond laser ablation. Geochim. Cosmochim. Acta 73, 5343–5360.

Steinhoefel, G., von Blanckenburg, F., Horn, I., Konhauser, K.O., Beukes, N.J., Gutzmer, J., 2010. Deciphering formation processes of banded iron formations from the Transvaal and the Hamersley successions by combined Si and Fe isotope analysis using UV femtosecond laser ablation. Geochim. Cosmochim. Acta 74, 2677–2696.

Stordal, M.C., Wasserburg, G.J., 1986. Neodymium isotopic study of Baffin bay water: Sources of REE from very old terranes. Earth Planet. Sci. Lett. 77, 259–272.

Tian, Y.Q., Yuan, G.P., Lu, J.R., Jing, Y., Yu, J.H., Li, M.M., 1986. Research on formation conditions and tectonic characteristics of Precambrian Yuanjiacun metamorphic-sedimentary iron deposits in Lan County. Geology and Mineral Resources Bureau Press, Shanxi, Shanxi Province.

Veizer, J., Compston, W., Hoefs, J., Nielsen, H., 1982. Mantle buffering of the early oceans. Naturwissenschaften 69, 173–180.

Viehmann, S., Hoffmann, J.E., Münker, C., Bau, M., 2014. Decoupled Hf–Nd isotopes in Neoarchean seawater reveal weathering of emerged continents. Geology 42, 115–118.

Wan, Y.S., Geng, Y.S., Shen, Q.H., Zhang, R.X., 2000. Khondalite series-geochrology and geochemistry of the Jiehekou Group in Lüliang area, Shanxi Province. Acta Petrol. Sin. 16, 49–58.

Wan, Y.S., Song, B., Liu, D.Y., Wilde, S.A., Wu, J.S., Shi, Y.R., Yin, X.Y., Zhou, H.Y., 2006. SHRIMP U–Pb zircon geochronology of Palaeoproterozoic metasedimentary rocks in the North China Craton: evidence for a major Late Palaeoproterozoic tectonothermal event. Precambrian Res. 149, 249–271.

Wang, C.L., Zhang, L.C., Lan, C.Y., Dai, Y.P., 2014a. Rare earth element and yttrium compositions of the Paleoproterozoic Yuanjiacun BIF in the Lüliang area and their implications for the Great Oxidation Event (GOE). Sci. Chin. Earth Sci. 57, 2469–2485.

Wang, C.L., Zhang, L.C., Liu, L., Dai, Y.P., 2014b. The formation era of BIF and its research methods. Chin. J. Geol. 49, 1201–1215.

Wang, C.L., Zhang, L.C., Dai, Y.P., Li, W.J., 2014c. Source characteristics of the ~2.5 Ga Wangjiazhuang banded iron formation from the Wutai greenstone belt in the North China Craton: evidence from neodymium isotopes. J. Asian Earth Sci. 93, 288–300.

Wang, C.L., Konhauser, K.O., Zhang, L.C., 2015a. Depositional environment of the Paleoproterozoic Yuanjiacun banded iron formation in Shanxi, China. Econ. Geol. 10, 1515–1539.

Wang, C.L., Zhang, L.C., Dai, Y.P., Lan, C.Y., 2015b. Geochronological and geochemical constraints on the origin of clastic meta-sedimentary rocks associated with the Yuanjiacun BIF from the Lüliang Complex, North China. Lithos 212–215, 231–246.

Xia, X.P., Sun, M., Zhao, G.C., Wu, F.Y., Xie, L.W., 2009. U–Pb and Hf isotopic study of detrital zircons from the Lüliang khondalite, Northe China Craton, and their tectonic implications. Geol. Mag. 146, 701–716.

Yu, J.H., Wang, D.Z., Wang, C.Y., 1997a. Geochemical characteristics and petrogenesis of the Early Proterozoic Bimodal Volcanic Rocks from Lüliang Group, Shanxi Province. Acta Petrol. Sin. 13, 59–70.

Yu, J.H., Wang, D.Z., Wang, C.Y., 1997b. Ages of the Lüliang group and its main metamorphism in the Lüliang mountains, Shanxi-evidence from single-grain zircon U–Pb ages. Geol. Rev. 43, 403–408.

Zhao, G.C., Sun, M., Wilde, S.A., Li, S.Z., 2005. Late Archean to Paleoproterozoic evolution of the North China Craton: key issues revisited. Precambrian Res. 136, 177–202.

Zhao, G.C., Wilde, S.A., Sun, M., Li, S.Z., Li, X.P., Zhang, J., 2008. SHRIMP U–Pb zircon ages of granitoid rocks in the Lüliang Complex: implications for the accretion and evolution of the Trans-North China Orogen. Precambrian Res. 160, 213–226.

Ziegler, K., Chadwick, O.A., Brzezinski, M.A., Kelly, E.F., 2005. Natural variations of δ^{30}Si ratios during progressive basalt weathering, Hawaiian Islands. Geochim. Cosmochim. Acta 69, 4597–4610.